Highly efficient second harmonic generation in hyperbolic metamaterial slot waveguides with large phase matching tolerance

Yu Sun,[1,2,*] Zheng Zheng,[2] Jiangtao Cheng,[3] Guodong Sun,[1] and Guofu Qiao[4]

[1]*School of Information Science and Technology, Beijing Forestry University, Beijing 100083, China*
[2]*School of Electronic and Information Engineering, Beihang University, Beijing 100191, China*
[3]*Department of Mechanical and Energy Engineering, University of North Texas, Denton, Texas 76207, USA*
[4]*School of Civil Engineering, Harbin Institute of Technology, Harbin 150006, China*
[*]*sunyv@bjfu.edu.cn*

Abstract: Highly efficient second harmonic generation (SHG) bridging the mid-infrared (IR) and near-IR wavelengths in a coupled hyperbolic metamaterial waveguide with a nonlinear-polymer-filled nanoscale slot is theoretically investigated. By engineering the geometrical parameters, the collinear phase matching condition is satisfied between the even hybrid modes at the fundamental frequency (3,100 nm) and the second harmonic (1,550 nm). Two modes manifest the great field overlap and the significant field enhancement in the nonlinear integration area (i.e. the slot), which leads to extreme large nonlinear coupling coefficient. For a low pumping power of 100 mW, the device length is as short as 2.19 μm and the normalized conversion efficiency comes up to more than 6.37×10^5 $W^{-1}cm^{-2}$ which outperforms that of the plasmonic-based structures. Moreover, the efficient SHG can be achieved with great phase matching tolerance, i.e., a small theoretical fabrication-error sensitivity to filling ratio and a broad pump bandwidth in a compact device length of 2.19 μm using 100 mW pump. The proposed scheme links the mature near-IR devices to the mid-IR regime and have a great potential for integrated chip-scale all-optical signal processes.

OCIS codes: (190.2620) Harmonic generation and mixing; (160.3918) Metamaterials; (190.4390) Nonlinear optics, integrated optics.

References and links

1. M. Ebrahim-Zadeh and I. T. Sorokina, *Mid-infrared Coherent Sources and Applications* (Springer, 2008).
2. R. A. Soref, S. J. Emelett, and W. R. Buchwald, "Silicon waveguided components for the long-wave infrared region," J. Opt. A, Pure Appl. Opt. **8**(10), 840–848 (2006).
3. E.-K. Tien, Y. Huang, S. Gao, Q. Song, F. Qian, S. K. Kalyoncu, and O. Boyraz, "Discrete parametric band conversion in silicon for mid-infrared applications," Opt. Express **18**(21), 21981–21989 (2010).
4. S. Zlatanovic, J. S. Park, S. Moro, J. M. C. Boggio, I. B. Divliansky, N. Alic, S. Mookherjea, and S. Radic, "Mid-infrared wavelength conversion in silicon waveguides using ultracompact telecom-band-derived pump source," Nat. Photonics **4**(8), 561–564 (2010).
5. X. Liu, B. Kuyken, G. Roelkens, R. Baets, R. M. Osgood, and W. M. J. Green, "Bridging the mid-infrared-to-telecom gap with silicon nanophotonic spectral translation," Nat. Photonics **6**(10), 667–671 (2012).
6. B. Jalali, "Silicon photonics: Nonlinear optics in the mid-infrared," Nat. Photonics **4**(8), 506–508 (2010).
7. J. Zhang, E. Cassan, and X. Zhang, "Efficient second harmonic generation from mid-infrared to near-infrared regions in silicon-organic hybrid plasmonic waveguides with small fabrication-error sensitivity and a large bandwidth," Opt. Lett. **38**(12), 2089–2091 (2013).
8. R. W. Boyd, *Nonlinear Optics* (Elsevier Science, 2008).
9. A. R. Davoyan, I. V. Shadrivov, and Y. S. Kivshar, "Quadratic phase matching in nonlinear plasmonic nanoscale waveguides," Opt. Express **17**(22), 20063–20068 (2009).
10. S. B. Hasan, C. Rockstuhl, T. Pertsch, and F. Lederer, "Second-order nonlinear frequency conversion processes in plasmonic slot waveguides," J. Opt. Soc. Am. B **29**(7), 1606–1611 (2012).

#228774 - $15.00 USD Received 28 Nov 2014; revised 30 Jan 2015; accepted 23 Feb 2015; published 2 Mar 2015

11. Z.- Wu, X.- Hu, Z.-y. Yu, W. Hu, F. Xu, and Y.- Lu, "Nonlinear plasmonic frequency conversion through quasiphase matching," Phys. Rev. B **82**(15), 155107 (2010).
12. F. F. Lu, T. Li, X. P. Hu, Q. Q. Cheng, S. N. Zhu, and Y. Y. Zhu, "Efficient second-harmonic generation in nonlinear plasmonic waveguide," Opt. Lett. **36**(17), 3371–3373 (2011).
13. J. Richter, A. Steinbrück, T. Pertsch, A. Tünnermann, and R. Grange, "Plasmonic core–shell nanowires for enhanced second-harmonic generation," Plasmonics **8**, 1–6 (2012).
14. W. Cai, A. P. Vasudev, and M. L. Brongersma, "Electrically controlled nonlinear generation of light with plasmonics," Science **333**(6050), 1720–1723 (2011).
15. J. Zhang, E. Cassan, D. Gao, and X. Zhang, "Highly efficient phase-matched second harmonic generation using an asymmetric plasmonic slot waveguide configuration in hybrid polymer-silicon photonics," Opt. Express **21**(12), 14876–14887 (2013).
16. A. Poddubny, I. Iorsh, P. Belov, and Y. Kivshar, "Hyperbolic metamaterials," Nat. Photonics **7**(12), 948–957 (2013).
17. V. P. Drachev, V. A. Podolskiy, and A. V. Kildishev, "Hyperbolic metamaterials: new physics behind a classical problem," Opt. Express **21**(12), 15048–15064 (2013).
18. D. Lu, J. J. Kan, E. E. Fullerton, and Z. Liu, "Enhancing spontaneous emission rates of molecules using nanopatterned multilayer hyperbolic metamaterials," Nat. Nanotechnol. **9**(1), 48–53 (2014).
19. G. A. Wurtz, R. Pollard, W. Hendren, G. P. Wiederrecht, D. J. Gosztola, V. A. Podolskiy, and A. V. Zayats, "Designed ultrafast optical nonlinearity in a plasmonic nanorod metamaterial enhanced by nonlocality," Nat. Nanotechnol. **6**(2), 107–111 (2011).
20. G. V. Naik, B. Saha, J. Liu, S. M. Saber, E. A. Stach, J. M. K. Irudayaraj, T. D. Sands, V. M. Shalaev, and A. Boltasseva, "Epitaxial superlattices with titanium nitride as a plasmonic component for optical hyperbolic metamaterials," Proc. Natl. Acad. Sci. U.S.A. **111**(21), 7546–7551 (2014).
21. H. N. S. Krishnamoorthy, Z. Jacob, E. Narimanov, I. Kretzschmar, and V. M. Menon, "Topological Transitions in Metamaterials," Science **336**(6078), 205–209 (2012).
22. Z. Liu, H. Lee, Y. Xiong, C. Sun, and X. Zhang, "Far-Field Optical Hyperlens Magnifying Sub-Diffraction-Limited Objects," Science **315**(5819), 1686 (2007).
23. D. R. Smith and D. Schurig, "Electromagnetic wave propagation in media with indefinite permittivity and permeability tensors," Phys. Rev. Lett. **90**(7), 077405 (2003).
24. X. Yang, J. Yao, J. Rho, X. Yin, and X. Zhang, "Experimental realization of three-dimensional indefinite cavities at the nanoscale with anomalous scaling laws," Nat. Photonics **6**(7), 450–454 (2012).
25. Y. He, S. He, J. Gao, and X. Yang, "Nanoscale metamaterial optical waveguides with ultrahigh refractive indices," J. Opt. Soc. Am. B **29**(9), 2559–2566 (2012).
26. Y. He, S. He, and X. Yang, "Optical field enhancement in nanoscale slot waveguides of hyperbolic metamaterials," Opt. Lett. **37**(14), 2907–2909 (2012).
27. Y. Enami, C. Derose, D. Mathine, C. Loychik, C. Greenlee, R. Norwood, T. Kim, J. Luo, Y. Tian, A.-Y. Jen, and N. Peyghambarian, "Hybrid polymer/sol–gel waveguide modulators with exceptionally large electro–optic coefficients," Nat. Photonics **1**(3), 180–185 (2007).
28. V. Agranovich and V. Kravtsov, "Notes on crystal optics of superlattices," Solid State Commun. **55**(1), 85–90 (1985).
29. P. B. Johnson and R.-W. Christy, "Optical constants of the noble metals," Phys. Rev. B **6**(12), 4370–4379 (1972).
30. E. D. Palik, *Handbook of Optical Constants of Solids, Volumes I, II, and III: Subject Index and Contributor Index* (Elsevier Science & Tech, 1985).
31. Z. Ruan, G. Veronis, K. L. Vodopyanov, M. M. Fejer, and S. Fan, "Enhancement of optics-to-THz conversion efficiency by metallic slot waveguides," Opt. Express **17**(16), 13502–13515 (2009).
32. Y. Bian, Z. Zheng, X. Zhao, J. Zhu, and T. Zhou, "Symmetric hybrid surface plasmon polariton waveguides for 3D photonic integration," Opt. Express **17**(23), 21320–21325 (2009).
33. Y. Bian, Z. Zheng, Y. Liu, J. Liu, J. Zhu, and T. Zhou, "Hybrid wedge plasmon polariton waveguide with good fabrication-error-tolerance for ultra-deep-subwavelength mode confinement," Opt. Express **19**(23), 22417–22422 (2011).
34. K. R. Parameswaran, R. K. Route, J. R. Kurz, R. V. Roussev, M. M. Fejer, and M. Fujimura, "Highly efficient second-harmonic generation in buried waveguides formed by annealed and reverse proton exchange in periodically poled lithium niobate," Opt. Lett. **27**(3), 179–181 (2002).

1. Introduction

Mid-infrared (IR), defined as wavelengths from 2 μm to 6 μm, has great potentials in chemical and bio-molecular sensing, free space communication, and thermal imaging for both civil and military purposes [1–3]. Yet, sources and detectors comparable to those in the near-IR regime have not yet emerged in this wavelength range [4]. To bridge the mid-IR to near-IR gap, novel devices based on four wave mixing and second harmonic generation (SHG) are theoretically conceived and experimentally demonstrated [3, 5–7]. However, the conversion efficiency may be increased by using lower-order nonlinear processes with larger nonlinear

#228774 - $15.00 USD Received 28 Nov 2014; revised 30 Jan 2015; accepted 23 Feb 2015; published 2 Mar 2015

susceptibilities [8]. The surface plasmon polarizations (SPPs) enable light confinement beyond diffraction limit and field enhancement of localized intensities, which facilities the nonlinear processes remarkably. The SHG has been presented in plasmonic slot waveguides [9, 10], long-range plasmonic waveguides [11], hybrid plasmonic waveguides [12] and plasmonic core-shell nanowires [13]. A promising way of further improving the conversion efficiency is the integration of plasmonic-based structures and the organic polymer with large nonlinear susceptibilities [8]. For example, the electrically controlled second harmonic generation (SHG) in plasmonic slot with polymers was demonstrated experimentally in [14]. More recently, efficient SHG in silicon-organic hybrid plasmonic waveguides with large phase mismatch tolerance [7] and in nonlinear polymer infiltrated plasmonic slot waveguide with normalized conversion efficiency above 1.3×10^5 $W^{-1}cm^{-2}$ [15] are theoretically investigated.

The hyperbolic metamaterials (HMs), which are consisted of layered metal-dielectric structures or nanowire arrays, have drawn significant interest very recently [16–22]. The HM display open-curved hyperbolic dispersion, which originates from one of the principal components of their electric effective tensor having the opposite sign to the other two [23]. Extremely large wave vectors are supported in the HM due to the unbound hyperbolic dispersion [24]. The giant momentum mismatch between the HM and air results in total internal reflection at the interfaces [24, 25]. So the HM waveguide enables the deep sub-wavelength confinement with ultrahigh effective index [25], which exceeds those of traditional plasmonic-based structures. Due to the normal electric displacement continuity, significant electric field enhancement occurs at the low-index slot region of the coupled HM waveguides [26]. In contrary, nonlinear optical processes associated with HMs remain relatively unexplored compared with their linear counterparts.

To further increase the efficiency of SHG, reduce the power consumptions and scale down the footprints, HM-based devices are the most promising candidates. A coupled HM waveguide with a nonlinear-polymer-filled nanoscale slot is proposed in this work for efficient SHG. The hybridization of two coupled HM waveguides enhances the optical field dramatically within the polymeric slot, which opens up opportunities for further improving the performance of nonlinear processes under low pumping power in short propagation distance. Based on this HM slot waveguide, we theoretically investigated the second-order wavelength conversion between the mid-IR (3,100 nm) and the near-IR (1,550 nm). Both the great field overlap and the significant field enhancement in the polymeric slot facilitate the nonlinear wavelength conversion. The normalized conversion efficiency is studied with different pumping powers and efficient SHG can be achieved with great phase matching tolerance, i.e., a small theoretical fabrication-error sensitivity to filling ratio and a broad bandwidth in a device of less than 2.3 μm long. For a low pumping power of 100 mW, the device length is as short as 2.19 μm and the normalized conversion efficiency reaches more than 6.37×10^5 $W^{-1}cm^{-2}$ which exceeds that in plasmonic-based structures. The proposed waveguide have a great potential for integrated all-optical signal processes.

#228774 - $15.00 USD Received 28 Nov 2014; revised 30 Jan 2015; accepted 23 Feb 2015; published 2 Mar 2015

2. Waveguide structure and design procedure

2.1 waveguide structure

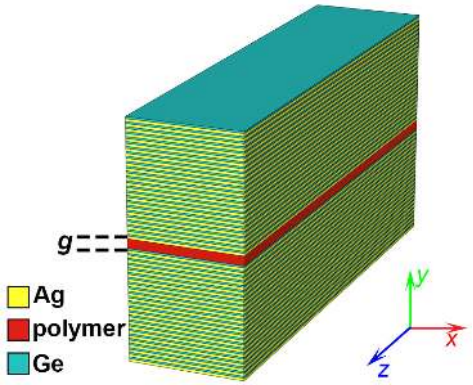

Fig. 1. Schematic of the proposed waveguide with a nonlinear-polymer-filled nanoscale slot.

The Fig. 1 shows the schematic of the proposed HM slot waveguides. Two identical HM waveguides composed of alternating metal-dielectric multi layers [25, 26] with a square cross section of 250 nm × 250 nm are placed adjacent to the both sides of a nonlinear organic polymer in the slot (height g = 20 nm). The assumed polymer is a doped, cross-linked organic polymer with a nonlinear susceptibility of $\chi^{(2)}_{111}$ = 619 pm/V [15, 27] and refractive index n = 1.68 at the wavelength of λ = 1,550 nm (n = 1.58 at λ 3,100 nm) [24]. The hyperbolic metamaterials were composed by alternate thin layers of silver (Ag, filling ratio f_r) and germanium (Ge) with a pitch thickness of 10 nm [24]. The metamaterial can be treated as a homogeneous effective medium [25, 26]. The linear modal properties taking into the nonlinear coupling wave equations are the complex effective index and the field distribution in the slot. The difference between these two properties derived from the effective medium approximation and the multi-layer structures are less than 1%. The principle components of the anisotropic permittivity tensor are given by [28]:

$$\varepsilon_x = \varepsilon_z = f_r \varepsilon_{Ag} + (1 - f_r)\varepsilon_{Ge}$$
$$\varepsilon_y = \frac{\varepsilon_{Ag}\varepsilon_{Ge}}{f_r \varepsilon_{Ge} + (1 - f_r)\varepsilon_{Ag}} \quad . \tag{1}$$

The permittivity of Ag ε_{Ag} is derived from the Drude model:

$$\varepsilon_{Ag}(\omega) = \varepsilon_\infty - \omega_p^2 / (\omega^2 + i\omega\gamma), \tag{2}$$

with a background dielectric constant ε_∞ = 5, plasma frequency ω_p = 1.38 × 10^{16} rad/s, and collision frequency γ = 5.07 × 10^{13} rad/s [29]. The permittivity of Ge ε_{Ge} is described by [30]:

$$\varepsilon_{Ge} = 9.28156 + 6.72880\lambda^2 / (\lambda^2 - 0.44105) + 0.21307\lambda^2 / (\lambda^2 - 3870.1). \tag{3}$$

By tuning filling ratio f_r and the operation wavelength, one can attain the hyperbolic regime when $\varepsilon_x = \varepsilon_z < 0$ and $\varepsilon_y > 0$.

#228774 - $15.00 USD Received 28 Nov 2014; revised 30 Jan 2015; accepted 23 Feb 2015; published 2 Mar 2015

2.2 Phase match condition and nonlinear coupling coefficient

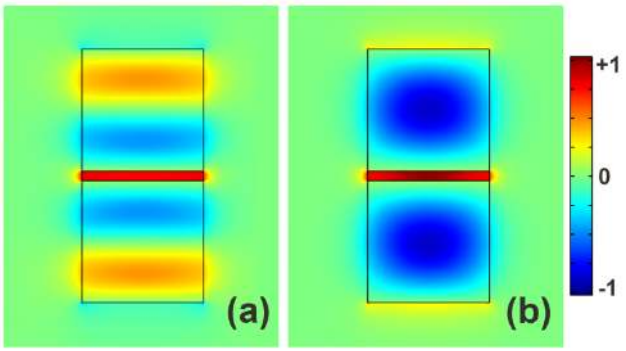

Fig. 2. The E_y profiles of (a) EHM(1,2) at 3,100 nm, (b) EHM(1,1) at 1,550 nm with f_r = 0.57 using the effective medium approximation.

To increase the SHG efficiency in terms of higher conversion yield and smaller device footprint, we need to increase nonlinear coupling coefficients (NCC) and reduce propagation attenuation while satisfying the phase matching condition [31]. The first key factor under consideration is the NCC between the interacting modes. The improper spatial overlap between modes with different concentrations or different symmetries will result in small NCC, which inevitably leads to a poor SHG efficiency. The electric field of the guided mode propagating along the + *z* direction can be expressed in the following form [31]:

$$e(x,y,z) = A(z)E(x,y)\exp[(\beta + i*\alpha/2)z], \tag{4}$$

where *A(z)* is the slowly varying complex mode amplitudes, *E(x, y)* is the normalized modal profile. The wave number $\beta = 2\pi \,\mathrm{Re}(n_{eff})/\lambda$ and the attenuation coefficient $\alpha = 4\pi \,\mathrm{Im}(n_{eff})/\lambda$ are derived from the complex effective index n_{eff} calculated from the commercial finite-element-method solver COMSOL™. Then the NCC $\kappa_{1,2}$ is defined as [15]:

$$\begin{aligned} \kappa_1 &= \varepsilon_0 \iint [\chi^{(2)} : E_{SH}(x,y) E^*_{FF}(x,y) \cdot E'_{FF}(x,y)] dxdy \\ \kappa_2 &= \varepsilon_0 \iint [\chi^{(2)} : E_{FF}(x,y) E_{FF}(x,y) \cdot E'_{SH}(x,y)] dxdy, \end{aligned} \tag{5}$$

where *E'(x, y)* is the normalized mode profile of the corresponding guided mode that propagates along opposite direction. The subscripts SH and FF represent the second harmonic (1,550 nm) and the fundamental frequency (3,100 nm), respectively.

For the mode order (m_x, m_y), m_x and m_y represent the number of peaks in the principal component of the electric field inside the individual HM waveguide along the *x* and *y* direction, respectively. The proposed HM slot waveguide supports the even hybridization of individual modes. The even hybrid modes (EHMs) not only inherit all of the advantages of individual modes listed above but also present some unique features [26], such as a greatly enhanced field in the low-index polymeric slot due to the slot effect [32, 33]. To make the most use of the material nonlinearity, the EHMs with m_x = 1 exhibiting a zero phase accumulation (a constant phase) along the *x* direction [25] are preferred.

Since high-order modes tend to have a larger mode index, which leads to higher absorption losses due to tighter field confinement [25]. The EHMs with lower m_x and m_y are preferred for reducing propagation attenuation. Considering the mode overlap and propagation attenuation, the lowest two order EHMs(m_x = 1, m_y) with m_y = 1 for SH and m_y = 2 for FF are selected for SHG. Modal profiles of the *y* component of the electric fields according to the coordinate frame shown in Fig. 1 for the two modes are depicted in Fig. 2.

#228774 - $15.00 USD Received 28 Nov 2014; revised 30 Jan 2015; accepted 23 Feb 2015; published 2 Mar 2015

The proposed waveguide displays normal dispersion because of the opposite signs of the principal components of the permittivity tensor in HM [24, 25]. So it is noteworthy that the FF signal with longer wavelength propagates in the higher order mode. The modal profiles shown in Fig. 2 indicate significant field enhancement and field overlap without cancellation in the nonlinear integration area (i.e. the slot). The NCC values are $\kappa_1 = \kappa_2^* = 4.54\text{x}10^3$ ps/m/W$^{1/2}$ at the filling ratio of $f_r = 0.57$. Compared with silicon-organic hybrid plasmonic waveguide [7] and organic plasmonic slot waveguide [15], more than an order of magnitude improvement in NCC is achieved in the proposed waveguide.

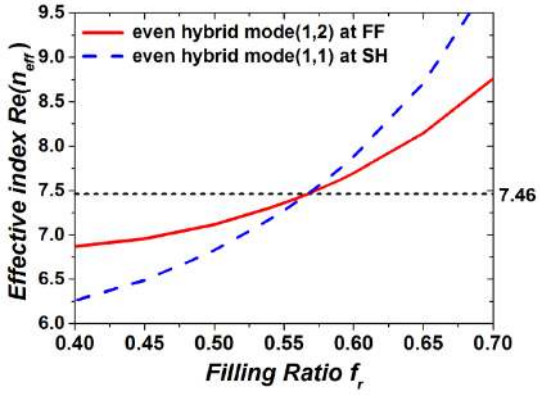

Fig. 3. The effective index Re(n_{eff}) as a function of the filling ratio f_r using the effective medium approximation.

The phase mismatch in SHG is defined as: $\Delta\beta = \beta_{SH} - 2\beta_{FF}$ [7, 15]. At the phase match point ($\Delta\beta = 0$), the second-order polarization and the generated harmonic propagate with the same phase velocity. By engineering the geometrical parameters of the proposed waveguide, phase match can be satisfied between EHM(1,2) at FF and EHM(1,1) at SH. The Fig. 3 illustrates the effective index Re(n_{eff}) as functions of filling ratio f_r. The cross point in Fig. 3 indicates a phase match point between two modes at different frequencies. Though there are other modes at SH near EHM(1,1) in term of their effective indices, the SHG to these modes is negligible due to either tiny NCC or great phase mismatch. At this point ($f_r = 0.57$), the complex effective index n_{eff} of the EHM(1,2) at FF and EHM(1,1) at SH are 7.462.0.151i and 7.463 + 0.071i, respectively.

3. SHG performance in the proposed waveguide

3.1 SHG efficiency

The SHG process in the proposed hybrid structure is investigated numerically by solving the nonlinear coupling wave equations for lossy waveguides [15, 31]:

$$\begin{aligned}\frac{\partial \mathrm{A_{FF}}}{\partial z} &= -\frac{\alpha_{FF}}{2}\mathrm{A_{FF}} + i\frac{\omega}{4}\kappa_1 A_{FF}^{*} A_{SH}\exp(i\Delta\beta z)\\ \frac{\partial \mathrm{A_{SH}}}{\partial z} &= -\frac{\alpha_{SH}}{2}\mathrm{A_{SH}} + i\frac{\omega}{4}\kappa_2^{*} A_{FF} A_{FF}\exp(-i\Delta\beta z).\end{aligned} \tag{6}$$

To evaluate the efficiency of SHG, a normalized conversion efficiency [34] is defined as the factor of merit:

$$\eta = \frac{P_{SH}(L_P)}{P_{FF}(0)^2 L_p^2}, \tag{7}$$

#228774 - $15.00 USD Received 28 Nov 2014; revised 30 Jan 2015; accepted 23 Feb 2015; published 2 Mar 2015

where $P_{FF}(0)$ is the pumping power of the FF, L_p is the length when the generated SH reaches its maximum and $P_{SH}(L_p)$ is the corresponding maximum output power, respectively. A pump power of 1 W was considered to make a direct comparison with the previous work [10, 15]. The Fig. 4(a) shows the SHG conversion process along propagation of 10 μm given a FF pump power of 1 W (30 dBm). The power of the FF signal decreases monotonously due to the nonlinear conversion and propagation loss, while the power of the SH signal ramps up quickly as a result of the efficient energy feeding from FF through frequency doubling. Due to the phase match between the FF and SH modes, the SH signal builds up coherently without oscillation over the entire length of waveguide. The SH signal reaches its maximum power up to 190.8 mW at a propagation distance of only 1.62 μm. The corresponding normalized conversion efficiency is 7.26×10^6 $W^{-1}cm^{-2}$.

Although the plasmonic slot waveguide manifests stronger field enhancement, the different symmetric of FF and SH modes involving in SHG seriously degrades the performance. The field enhancement improves with reduced slot separation, but the anti-symmetric still exists between the 1st mode at SH and 0th mode at FF in plasmonic slot waveguide [15]. The cancellation significantly reducing the NCC can only be mitigated in plasmonic slot waveguide, while it can be completely avoided in HM slot waveguide. Considering the same slot separation of 20 nm, our scheme still outperform that in [15] more than 6 times in term of normalized conversion efficiency.

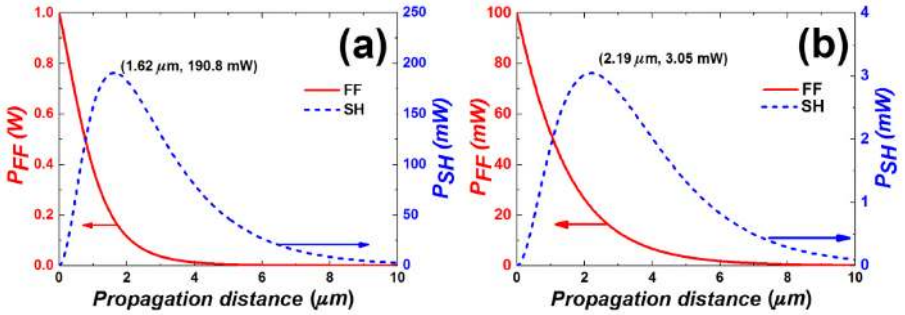

Fig. 4. Optical powers of the FF and SH waves as a function of the propagation distance pumped by (a) 1W and (b) 100mW.

Low pump power is highly desirable in optical operations of various nonlinear applications of integrated photonic circuits. Since the proposed waveguide has such a large NCC, the SHG can be efficiently generated under a pump power as low as 100 mW (20 dBm). As indicated in Fig. 4(b), the peak power of the generated SH signal reached as high as 3.05 mW at a propagation length of only 2.19 μm. The corresponding normalized conversion efficiency is 6.37×10^5 $W^{-1}cm^{-2}$, which is 5 times higher than that of metallic plasmonic slot waveguide pumped by the same power [15].

#228774 - $15.00 USD Received 28 Nov 2014; revised 30 Jan 2015; accepted 23 Feb 2015; published 2 Mar 2015

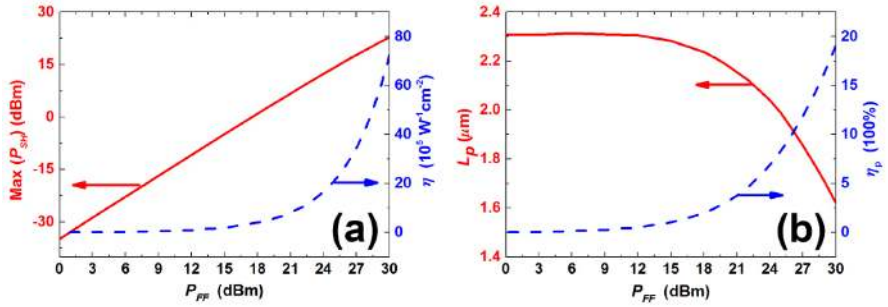

Fig. 5. The (a) maximum of SH power max(P_{SH}), normalized conversion efficiency η, (b) peak position L_p and peak efficiency η_p as a function of the input pumping power P_{FF}.

The SHG bridging the gap between the mid-IR and near-IR wavelengths is then investigated under various pump powers. Figure 5 shows the maximum SH power, normalized conversion efficiency, peak position and peak efficiency as a function of the pump power. The peak efficiency is defined as:

$$\eta_p = \frac{P_{SH}(L_P)}{P_{FF}(0)}, \tag{8}$$

As expected, the maximum of SH power increases monotonously with the pump power. As indicated in Fig. 5, both the normalized conversion efficiency and the peak efficiency are greatly affected by the pump power while the peak length remains shorter than 2.3 μm in all cases. It is noteworthy that the peak efficiency remains ~5% with the pump power as low as 12 dBm, indicating that a continuous wave output of SH is possible. This dramatic improvement makes the proposed waveguide very promising and competitive for low-power all-optical nonlinear applications.

3.2 theoretical fabrication-error tolerance and conversion bandwidth

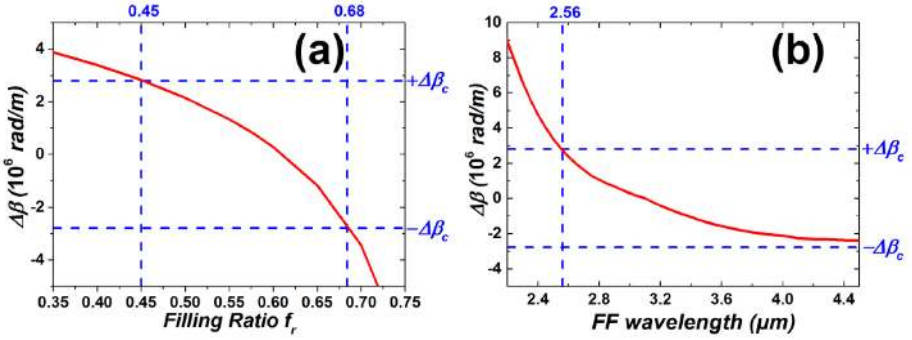

Fig. 6. The phase mismatch as functions of (a) filling ratio f_r and (b) wavelength of the FF.

With a given device length L, the related phase matching tolerance can be written as [8]:

$$|\Delta\beta| < \Delta\beta_c \equiv 2\pi/L, \tag{9}$$

With L = 2.19 μm (considering a pump power of 100 mW), the $\Delta\beta_c$ is 2.87 × 10^6 rad/m. The Fig. 6 shows the phase mismatch between the EHM(1,2) at the FF and EHM(1,1) at the SH as a function of the filling ratio f_r and the FF wavelength. Due to the ultra-short device length, the phase matching tolerance is satisfied for a wide range of filling ratio (0.45 ~0.68) and a wide band of wavelengths (2.56 μm ~> 4 μm). The wavelength tuning requirements are very

#228774 - $15.00 USD Received 28 Nov 2014; revised 30 Jan 2015; accepted 23 Feb 2015; published 2 Mar 2015

relaxed and therefore the proposed waveguide allows a coherent buildup of SHG in ultra-wideband.

4. Conclusions

In conclusion, we have proposed a coupled hyperbolic metamaterial waveguide with a nonlinear-polymer-filled nanoscale slot. Taking the mode profile overlap and propagation loss into consideration, the EHM(1,2) at 3,100 nm and EHM(1,1) at 1,500 nm are selected for second harmonic generation. Both the great field overlap and the significant field enhancement in the polymeric slot facilitate the nonlinear wavelength conversion. By engineering the geometrical parameters, the collinear phase matching condition is satisfied between the modes of interest with a large nonlinear coupling coefficient. The second harmonic generation bridging the mid-IR and near-IR wavelengths is then theoretically investigated under various pump powers. Our analysis indicates that the device length can be as short as several micrometers and the normalized conversion efficiency can be two orders of magnitude higher than that of a plasmonic slot waveguide. Moreover, high-efficiency second harmonic generation can be achieved with great phase matching tolerance, i.e., a smaller theoretical fabrication-error sensitivity to filling ratio and a broader pump bandwidth due to the ultra-short conversion distance. The proposed device exhibits great potential for integrated chip-scale all-optical signal processing with low pump power and high phase mismatch tolerance.

Acknowledgments

This work was supported by the Fundamental Research Funds for the Central Universities (BLX2014-26 / TD2014-01), 973 Program (2012CB315601) and NSFC (61435002 / 51328601 / 61107057 / 61221061 / 61300180 / 51378156).

#228774 - $15.00 USD Received 28 Nov 2014; revised 30 Jan 2015; accepted 23 Feb 2015; published 2 Mar 2015